SCIENCE CHINA Chemistry



·ARTICLES·

March 2025 Vol.68 No.3: 974–979 https://doi.org/10.1007/s11426-024-2280-8

Boosting photocatalytic CO₂-to-CO conversion using a biomimetic dinuclear Co(II) complex through an HCO₃-mediated pathway

Yuchen Wang, Wenjie Shi*, Weixue Tao, Jihong Zhang, Di-Chang Zhong* & Tongbu Lu*

Institute for New Energy Materials and Low Carbon Technologies, School of Materials Science and Engineering, Tianjin University of Technology, Tianjin 300384, China

Received July 22, 2024; accepted August 27, 2024; published online November 15, 2024

Dinuclear metal synergistic catalysis (DMSC) has been evidenced to be effective in enhancing the catalytic activity for CO_2 reduction. However, the reaction kinetics of CO_2 reduction is still limited by the local CO_2 concentration around the dinuclear catalytic centers. Inspired by the structure of carbonic anhydrase, we have designed and synthesized a dinuclear cobalt(II) complex with an –OH group. This complex not only exhibits DMSC for CO_2 reduction but also possesses excellent capture capacity for CO_2 molecules. Consequently, the complex demonstrates high efficiency for the photocatalytic reduction of CO_2 to CO_2 , with turnover number reaching as high as 43,400 and a selectivity of 97%. Even in 10% CO_2 , the complex still shows state-of-the-art catalytic activity. The results of experiments and theoretical calculations reveal that besides the DMSC contributing to the enhanced catalytic activity, the –OH group in the dinuclear cobalt(II) complex facilitates the capture of CO_2 by the formation of HCO_3^- intermediates, thereby enhancing the affinity towards CO_2 and boosting the catalytic activity for CO_2 -to-CO conversion.

homogeneous catalyst, dinuclear metal synergistic catalysis, CO₂ reduction, photocatalysis, enzyme mimics

Citation: Wang Y, Shi W, Tao W, Zhang J, Zhong DC, Lu T. Boosting photocatalytic CO₂-to-CO conversion using a biomimetic dinuclear Co(II) complex through an HCO₃-mediated pathway. Sci China Chem, 2025, 68: 974–979, https://doi.org/10.1007/s11426-024-2280-8

1 Introduction

Utilization of solar energy to drive the reduction of carbon dioxide (CO₂) into fuels or valuable chemicals is an auspicious approach to tackle the prevailing energy crisis and environmental challenges [1–8]. Recent research has evidenced that the dinuclear metal synergistic catalysis (DMSC) effect between two metal sites in dinuclear metal complexes is effective in enhancing the photocatalytic activity of CO₂ reduction [9–11]. Consequently, designing and synthesizing dinuclear metal complexes with the DMSC effect offers a promising strategy to develop high-efficiency catalysts for photocatalytic CO₂ reduction. To further enhance the reac-

tion kinetics of photocatalytic CO_2 reduction by dinuclear metal complexes, enhancing the affinity of the dinuclear catalytic center with CO_2 molecules would be effective. The chemisorption of CO_2 molecules [12–15] is generally considered an important prerequisite for the occurrence of photocatalytic CO_2 reduction [16–20].

In nature, carbonic anhydrase (CA) is an ancient metalloenzyme that catalyzes the hydration of CO₂ to form bicarbonate, showing exceptional CO₂ absorption capability [21–24]. This is attributed to the core structure of N₃ZnOH, where the Zn(II) in a tetrahedral geometry coordinates with three histidine groups and a –OH group (Figure 1a). The –OH group acts as a nucleophile reacting with CO₂ to form bicarbonate, thus facilitating the CO₂ capture [25]. Inspired by the scaffold of CA, we tried to design and synthesize dinuclear metal complexes with –OH groups around the

^{*}Corresponding authors (email: wjshi@email.tjut.edu.cn; dczhong@email.tjut.edu.cn; lutongbu@tjut.edu.cn)

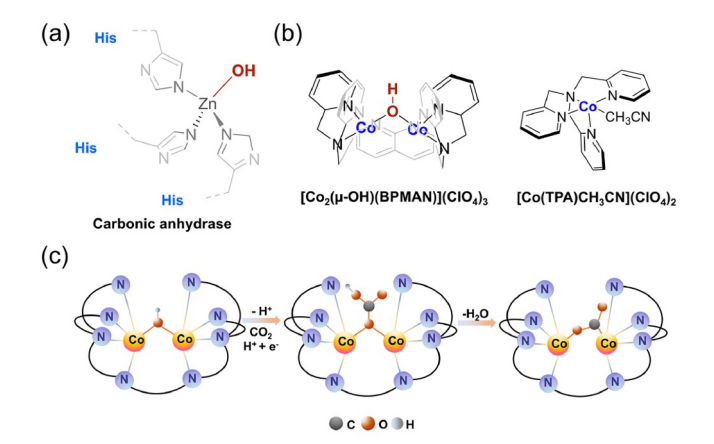


Figure 1 (Color online) Structures of (a) carbonic anhydrase and (b) $[Co_2-(\mu-OH)(BPMAN)](CIO_4)_3$ (1), $[Co(TPA)CH_3CN](CIO_4)_2$ (2). (c) The proposed CO_2 adsorption pathway for 1 in the CO_2 reduction process.

dinuclear metal center for photocatalytic CO₂ reduction.

Herein, we report a Co(II) complex of [Co₂(μ-OH)- $(BPMAN)](ClO_4)_3$ (1; BPMAN = 2,7-[bis(2-pyridylme-thyl)aminomethyl]-1,8-naphthyridine) with the above-mentioned structural features (Figure 1b) [26,27]. That is, firstly, the N atoms in BPMAN are capable of coordinating two Co(II) ions with an M...M distance of 3.3 Å, which aligns with the ideal range for generating DMSC effect for CO2 reduction (Figure S1, Supporting Information online) [28–30]. Secondly, a –OH group positioned between the dinuclear Co(II) centers in BPMAN offers a potential bicarbonate (HCO₃⁻) pathway for CO₂ adsorption (Figure 1c), mimicking the function of the -OH group in CA for capturing CO₂ molecules. As expected, 1 shows remarkable efficiency in the photocatalytic reduction of CO₂ to CO, achieving a maximum turnover number (TON) as high as 43,400 and a selectivity of 97%, which surpasses its monometallic counterpart by a significant margin. Furthermore, 1 also demonstrates state-of-the-art photocatalytic activity in 10% CO₂. The results of experiments and density functional theory (DFT) calculation reveal that the –OH groups in 1 significantly promote the CO₂ adsorption process via an HCO₃ pathway, which works together with the DMSC, greatly enhancing the photocatalytic activity for CO₂ reduction. These findings not only highlight the efficacy of the DMSC in boosting CO₂ reduction but also underscore the utility of strengthening CO₂ adsorption for promoting the reaction kinetics of CO2 reduction, thereby giving new insights for developing efficient catalysts for CO₂ reduction.

2 Experimental

2.1 Materials

All chemicals and materials were commercially obtained from Energy Chemical, Aladdin and Adamas-beta, and used without further purification. All gases were purchased from Tianjin Huanyu Gas and the purity of argon and carbon dioxide was 99.999%. The ultraviolet-visible spectra (UV-vis) were obtained by a UV-vis spectrophotometer (UV-3600, Shimadzu, Japan). The photoluminescence (PL) spectra were conducted on a fluorescence spectrophotometer (F-7000, Hitachi, Japan). In situ Fourier transform infrared (FTIR) spectra in the 650-4,000 cm⁻¹ region were collected on a Nicolet iS50 FTIR spectrometer using KBr pellets. The isotopic labeling experiments were conducted under a ¹³CO₂ atmosphere and the gas products were analyzed by a quantitative mass spectrometer (HPR-20 Q/C Benchtop Gas Analysis System). The products in the gaseous phase of the reaction system were analyzed by a gas chromatograph (GC-2014+ATF, 230C, Shimadzu, Japan) equipped with two automated gas sampling valves, which contain a thermal conductivity detector (TCD) and a flame ionization detector (FID). The products in the liquid phase of the reaction system were analyzed by an ion chromatograph (DX-600, Dionex, USA) and a nuclear magnetic resonance spectrometer (AVANCE III HD 400 MHz).

2.2 Syntheses

Synthesis of 1. Under an Ar atmosphere, an CH_3OH solution (5 mL) of BPMAN (27.60 mg, 0.05 mmol) was added to an CH_3OH solution of $Co(CIO_4)_2 \cdot 6H_2O$ (45.80 mg, 0.13 mmol). The mixture was stirred at room temperature overnight. The resultant solution was concentrated to 2 mL under reduced pressure, washed with ethyl ether and dried under vacuum to give a brown powder (0.063 g, 87%).

Synthesis of **2**. TPA (0.42 g, 1.43 mmol) and Co(ClO₄)₂· 6H₂O (0.52 g, 1.42 mmol) were dissolved in 30 mL de-aerated CH₃CN. Then the resulting mixture was stirred for 30 min. Later, 100 mL deaerated ether was slowly added into the above solution and stood overnight. The resulting purple microcrystalline product was filtered, washed with ether (10 mL) and dried in a vacuum oven for 48 h (0.74 g, 79%).

3 Results and discussion

The ligands of 2,7-[bis(2-pyridylme-thyl)aminomethyl]-1,8-naphthyridine) (BPMAN) and tris(2-pyridylmethyl)amine (TPA) were synthesized according to literatures (Figures S2 and S3) [31–34]. The complex of $[Co_2(\mu\text{-OH})(BPMAN)]$ -(ClO₄)₃ (1) was synthesized through the combination of $Co(ClO_4)_2 \cdot 6H_2O$ with BPMAN ligand in CH₃OH solution. The liquid chromatography mass spectrometry (LC-MS) analysis revealed an ion peak at m/z 229.047, which corresponds to the presence of $[Co_2(\mu\text{-OH})(BPMAN)]^{3+}$ (Figure S4). The infrared (IR) spectroscopy of 1 in attenuated total reflection (ATR) mode showed remarkable peaks in the

range of 3,000–3,600 cm⁻¹, whereas they are absent in that of BPMAN (Figure S5), further confirming the existence of the -OH groups in 1 [35,36]. The UV-vis spectrum of 1 exhibited visible-light adsorption centered around 506 nm, attributed to the d-d transition of Co²⁺ (Figure S6). Additionally, the analysis of inductively coupled plasma mass spectrometry (ICP-MS) determined the Co content in 1 to be 11.65 wt%, closely aligning with the theoretical value of 12.07 wt%. These results confirm that 1 has been successfully synthesized. Analogously, the mononuclear Co(II) complex of $[Co(TPA)CH_3CN](ClO_4)_2$ (2), as the counterpart of 1, was prepared by mixing Co(ClO₄)₂·6H₂O with TPA ligand in CH₃CN solution. LC-MS of 2 in CH₃CN revealed an ion peak at m/z 174.542, corresponding to $[Co(TPA)]^{2+}$ (Figure S7). This result illustrates that the mononuclear Co(II) complex of 2 has also been successfully synthesized.

Photocatalytic CO₂ reduction experiments were performed in 17.5 mL glass tubes at room temperature, containing 1 or 2 (catalyst), [Ru(phen)₃](PF₆)₂ (photosensitizer, 0.4 mM, Figure S8), 1,3-dimethyl-2-phenylbenzimidazoline (BIH, electron donors, 0.025 M) and triethanolamine (TEOA, electron donors, 0.3 M) in a mixture of 5 mL CO₂-saturated CH₃CN/ H₂O solution. The solution was bubbled with CO₂ for 30 min and then irradiated under visible light (300 W Xenon lamp with 420 nm cutoff). As expected, 1 shows good photocatalytic activity for CO₂ reduction. When the ratio of CH₃CN and H₂O was 3:2, the concentration of BIH was 0.025 M, and 1 achieved optimal performance (Figures S9 and S10). In this case, 66.24 µmol CO and 4.96 µmol H₂ were detected when 1 µM 1 was used (Figure 2a; Table 1, Entry 1), corresponding to the TON_{CO} of 13,248, and the selectivity of 93% to CO. There is no liquid product generated in the reaction system (Figure S11). Under the same conditions, the mononuclear Co(II) complex of 2 also shows photocatalytic activity for CO₂ reduction, where 7.47 µmol of CO was detected when 2 μM 2 was used, corresponding to the TON_{CO}

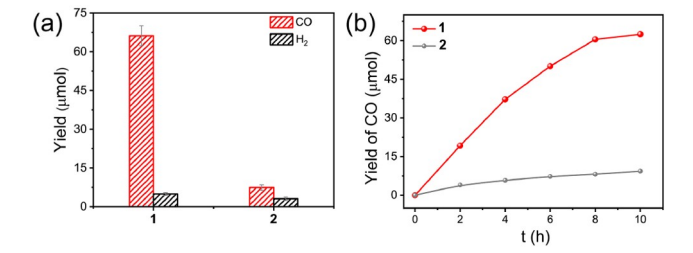


Figure 2 (Color online) (a) The photocatalytic CO_2 reduction activity of 1 and 2 (The data were repeated three times, with error bars shown). (b) Time profiles of CO and H_2 generation from the photocatalytic CO_2 reduction with 1 (1 μ M) and 2 (2 μ M).

of 747 (Figure 2a, b). Remarkably, the photocatalytic activity of 1 is much higher than that of 2, which illustrates there is a synergistic catalysis effect between two Co(II) centers in 1. The DMSC endows 1 with outstanding photocatalytic activity for CO_2 reduction to CO. The quantum yield of 1 for photocatalytic CO_2 reduction was determined to be 0.47% at 450 nm.

To further explore the activity of 1, the photocatalytic CO₂ reduction experiment by 1 at low concentrations was performed. It was found that even at 0.1 µM, a large amount of CO could still be detected (21.70 µmol), corresponding to the TON_{CO} of 43,400 (Table 1, Entries 2-4). The photocatalytic activity of 1 is comparable to those of reported dinuclear molecular catalysts (Table S1, Figure S12). The excellent photocatalytic activity of 1 was further evaluated under low CO₂ concentration. A mixed gas containing 10% CO₂ and 90% Ar to simulate the flue gas (5%–15% CO₂) was used in the photocatalytic system. The results show that 12.80 µmol of CO was produced after illumination for 10 h, corresponding to a TON_{CO} value of 2,560. Although the TON value of 1 in 10% CO₂ is lower than that in 100% CO₂, the value is still higher than that of most photocatalysts that perform in 100% CO₂ (Table S1) [37].

Table 1 Results of photocatalytic reduction of CO₂ to CO by 1

Entry	Cat (µM)	CO (µmol)	H ₂ (μmol)	CO (%)	TON _{CO}
1 ^{a)}	1.0	66.24	4.96	93	13,248
2	0.5	50.60	2.83	95	20,240
3	0.25	36.80	1.57	96	29,440
4	0.1	21.70	0.72	97	43,400
5 ^{b)}	0	1.46	0.25	84	291
6 ^{c)}	1.0	0.06	0	100	12
7 ^{d)}	1.0	0	0	0	100
8 ^{e)}	1.0	22.50	9.02	71	4,500
9 ^{f)}	1.0	0.89	0	100	178
10 ^{g)}	1.0	0	0	0	100

a) Reaction conditions: CH₃CN/H₂O (v/v = 3:2; 5.0 mL), [Ru(phen)₃](PF₆)₂ (0.4 mM), TEOA (0.3 M), BIH (0.025 M), 300 W Xe lamp ($\lambda > 420 \text{ nm}$), irradiation time = 10 h. b) Without catalyst. c) Without photosensitizer. d) Without irradiation. e) Without TEOA. f) Without BIH. g) In Ar.

A series of control experiments of CO₂ reduction by 1 were conducted to identify the role of each component in the photocatalytic system. The results indicate that only a trace amount of CO was detected without 1 (Table 1, Entry 5), and neither CO nor H₂ can be detected in the lack of [Ru(phen)₃]-(PF₆)₂ or illumination, demonstrating that the catalyst, photosensitizer, and light are all indispensable for the CO generation (Table 1, Entries 6-7). When cost-effective organic photosensitizers such as eosin, rhodamine B and pyrin were used instead of [Ru(phen)₃](PF₆)₂, no gaseous and liquidreduced product was detected. Additionally, when only TEOA or BIH was used, the generated CO was significantly reduced, which illustrates the importance of dual sacrificial agents for CO₂ reduction in this photocatalytic system (Table 1, Entries 8–9). To determine the source of the generated CO, Ar was used instead of CO₂. The result shows that no CO was detected in this case (Table 1, Entry 10). This observation illustrates that the generated CO originates from the CO₂ reduction. This conclusion was further evidenced by the isotope trace experiment. As shown in Figure S13, when ¹³CO₂ was used instead of CO₂, ¹³CO was generated in the photocatalytic system. All these results solidly support that the generated CO comes from CO2 rather than other components in the system.

The stability of 1 during the process of photocatalytic CO₂ reduction was investigated. It was observed that the rate of CO production almost stops after 10 h, and the addition of [Ru(phen)₃](PF₆)₂ and BIH can reactivate the CO₂-to-CO reaction (Figure S14), indicating that the cease of CO₂ reduction reaction is mainly attributed to the degradation of the photosensitizer (Figure S15) and/or the consumption of sacrificial agent. The UV-vis spectra of 1 in CH₃CN/H₂O solution remain basically unchanged after irradiation for 10 h (Figure S16), further confirming the durability of 1.

To well elucidate the different catalytic activity of 1 and 2 for CO₂ reduction, their electrochemical behavior was comprehensively analyzed. As illustrated in Figure S17, the cyclic voltammograms (CV) diagram of 1 in Ar shows one reduction wave at -0.74 V vs. NHE, which can be attributed to the reduction of Co₂(II,II) to Co₂(I,II). In addition, the catalytic current density for CO₂ reduction at -0.74 V vs. NHE increases linearly with the concentration of 1 (Figures S18 and S19), indicating a single site cobalt catalysis in 1 [9,38]. In contrast, the CV of 2 exhibits a primary reduction peak at -0.93 V vs. NHE, corresponding to the reduction of Co(II) to Co(I) (Figure S20). When the atmosphere was changed from Ar to CO₂, both 1 and 2 exhibited an increase in catalytic current density at their respective reduction waves, indicating their ability to catalyze CO₂ reduction. Moreover, the current density increase in 1 is obviously stronger than that of 2 at an identical Co(II) concentration. This finding underscores the superior catalytic activity of 1 over 2, well supports the experimental results of photo-

catalytic CO₂ reduction. In addition, to well understand the catalytic mechanism of 1 during the photochemical reduction of CO₂ to CO, quenching experiments of the excited $[Ru(phen)_3]^{2+*}$ by 1 and by the electron donor (BIH and TEOA) were carried out. As shown in Figures S21 and S22, the [Ru(phen)₃]²⁺ in the CH₃CN/H₂O exhibits a luminescence peak at 595 nm when excited at 450 nm. The excited [Ru(phen)₃]^{2+*} was dramatically quenched by BIH, and was not by 1 (Figures S23 and S24), indicating the excited [Ru(phen)₃]^{2+*} was quenched *via* a reductive quenching mode. This result suggests that the BIH firstly donates an electron to excited [Ru(phen)₃]^{2+*} to form [Ru(phen)₃]⁺. Then the formed [Ru(phen)₃]⁺ transfers the electron to the Co(II) center to generate Co(I). Finally, the Co(I) injects the electron into the adsorbed CO2 molecule to make CO2 reduction (Figure S25).

The process of photocatalytic CO_2 reduction by **1** was further monitored by using *in situ* FTIR spectroscopy. As shown in Figure 3a, four distinct peaks corresponding to the intermediates of HCO_3^- (1,392 and 1,219 cm⁻¹), *COOH (1,642 cm⁻¹), and *CO (2,078 cm⁻¹) are clearly identifiable, demonstrating that the adsorption of CO_2 onto the surface of **1** follows a *CO₃H pathway [39,40]. In addition, the formation of *CO occurs through the transformation of *COOH, by the process of *COOH + H⁺ + e⁻ \rightarrow *CO + H₂O [41–43].

Based on the above observations and results, a reasonable reaction pathway for the photocatalytic reduction of CO₂ to CO by 1 was proposed (Figure 3b), and further investigated by the density functional theory (DFT) calculation. Initially, the Lewis base -OH group in 1 facilitates the adsorption of CO₂, releasing a proton to form *CO₃ intermediate (Int-1). Later, the **Int-1** undergoes a proton-coupled electron transfer (PCET) process to form *CO₃H intermediate (Int-2), with the free energy change (ΔG) of 0.39 eV. Next, **Int-2** undergoes protonated and dehydration to yield *CO2 intermediate (Int-3). Then, the synergistic catalysis effect between two Co(II) sites promotes the conversion of Int-3 to undergo another PCET process, forming *CO-OH intermediate (Int-4). This process accelerates the C–O bond breaking and is exothermic, releasing 0.26 eV of energy. Following the release of CO ($\Delta G = -0.26 \text{ eV}$), 1 is regenerated and initiates the next catalytic cycle. While 2 follows the conventional CO2 adsorption pathway in the process of photocatalytic CO₂ reduction to CO (Figure S26). Notably, the above-calculated results show that for 1, the protonation of *CO₃H to form *CO₂ constitutes the ratedetermining step (RDS), with a lower ΔG of 1.16 eV compared to the RDS in 2, which involves the formation of a Co- CO_2 adduct with a ΔG of 1.44 eV (Figure 3c). The presence of the -OH group in 1 significantly strengthens the CO₂ adsorption and greatly boosts the photocatalytic CO₂ reduction to CO.

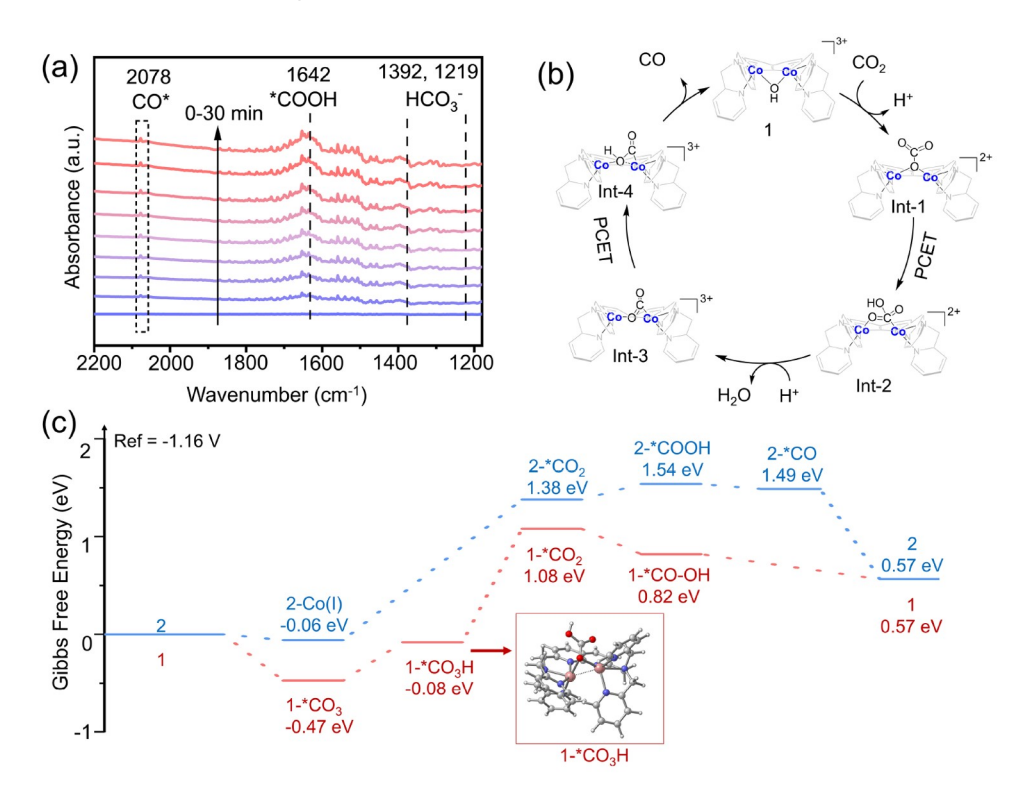


Figure 3 (Color online) (a) *In-situ* FTIR spectra of 1 during the process of photocatalytic CO₂ reduction. (b) Proposed catalytic mechanism of 1 for the reduction of CO₂-to-CO. (c) Energy diagram for CO₂ reduction catalyzed by 1 and 2.

4 Conclusions

In conclusion, inspired by the structure of carbonic anhydrase in nature, we have designed and synthesized a biomimetic dinuclear cobalt(II) complex incorporating an -OH group. Because of the synergistic catalysis of two Co(II), as well as the -OH groups facilitating the CO₂ adsorption, the dinuclear cobalt(II) complex possesses excellent activity for photocatalytic CO₂-to-CO conversion, showing impressively high TON_{CO} value of 43,400 and a selectivity of 97%, greatly outperforming its monometallic counterpart by a substantial margin. In this research, not only the design of dinuclear metal complexes with efficient catalytic activity for CO2 reduction has been achieved according to the DMSC concept, but also the strategy of introducing -OH groups to strengthen the CO₂ binding via forming an HCO₃ intermediate has been developed. These results give new insights for researchers in developing high efficiency catalysts for photocatalytic CO₂ reduction.

Acknowledgements This work was supported by the National Key R&D Program of China (2022YFA1502902), and the National Natural Science Foundation of China (22271218, 22071182, 22201209, and 21931007).

Conflict of interest The authors declare no conflict of interest.

Supporting information The supporting information is available online at chem.scichina.com and link.springer.com/journal/11426. The supporting materials are published as submitted, without typesetting or editing. The

responsibility for scientific accuracy and content remains entirely with the authors.

- Li D, Kassymova M, Cai X, Zang SQ, Jiang HL. Coord Chem Rev, 2020, 412: 213262
- 2 Zhang JH, Gong YN, Wang HJ, Wang YC, Yang W, Mei JH, Zhong DC, Lu TB. Proc Natl Acad Sci USA, 2022, 119: e2118278119
- 3 Zhong DC, Gong YN, Zhang C, Lu TB. Chem Soc Rev, 2023, 52: 3170–3214
- 4 Yuan H, Zhang M, Deng JH, Lu TB, Zhong DC. Sci China Chem, 2024, 67: 3712–3718
- 5 Ham R, Nielsen CJ, Pullen S, Reek JNH. Chem Rev, 2023, 123: 5225– 5261
- 6 Sun K, Qian Y, Jiang HL. Angew Chem Int Ed, 2023, 62: e202217565
- 7 Bharti J, Chen L, Guo Z, Cheng L, Wellauer J, Wenger OS, von Wolff N, Lau KC, Lau TC, Chen G, Robert M. J Am Chem Soc, 2023, 145: 25195–25202
- 8 Wang YM, Mo KM, Luo X, Xia RQ, Song JY, Ning GH, Li D. Sci China Chem, 2023, 66: 3525–3531
- Ouyang T, Huang HH, Wang JW, Zhong DC, Lu TB. Angew Chem Int Ed, 2017, 56: 738–743
- 10 Gong YN, Zhao SQ, Wang HJ, Ge ZM, Liao C, Tao KY, Zhong DC, Sakai K, Lu TB. Angew Chem Int Ed. 2024, 63: e202411639
- 11 Wang HF, Shi WJ, Yang YX, Dong BX, Lu TB, Zhong DC. Sci China Chem, 2024, doi: 10.1007/s11426-024-2108-2
- 12 Li GF, Zhu DX, Wang XL, Su ZM, Bryce MR. Chem Soc Rev, 2020, 49: 765–838
- 13 Cao LM, Huang HH, Wang JW, Zhong DC, Lu TB. *Green Chem*, 2018, 20: 798–803
- 14 Wu Y, Wu MY, Zhu JC, Zhang XJ, Li J, Zheng K, Hu J, Liu CY, Pan Y, Zhu JF, Sun YF, Xie Y. Sci China Chem, 2023, 66: 1997–2003
- 15 Zhang L, Li S, Liu H, Cheng YS, Wei XW, Chai X, Yuan G. *Inorg Chem*, 2020, 59: 17464–17472

- 16 Chen LL, Guo ZG, Wei XG, Gallenkamp C, Bonin J, Anxolabéhère-Mallart E, Lau KC, Lau TC, Robert M. J Am Chem Soc, 2015, 137: 10918–10921
- Hong DC, Kawanishi T, Tsukakoshi Y, Kotani H, Ishizuka T, Kojima T. J Am Chem Soc, 2019, 141: 20309–20317
- 18 Call A, Cibian M, Yamamoto K, Nakazono T, Yamauchi K, Sakai K. ACS Catal, 2019, 9: 4867–4874
- 19 Zhang BB, Sun LC. Chem Soc Rev, 2019, 48: 2216-2264
- 20 Zhang JH, Wang HJ, Shi WJ, Yang W, Mei JH, Wang YC, Lu TB, Zhong DC. CCS Chem, 2024, 1–10
- 21 Trogadas P, Xu LL, Coppens MO. Angew Chem Int Ed, 2024, 63: e202314446
- 22 Cobb SJ, Dharani AM, Oliveira AR, Pereira IAC, Reisner E. Angew Chem Int Ed, 2023, 62: e202218782
- 23 Ying Q, Chen H, Shao PJ, Zhou XW, He XJ, Ye JX, Zhang SH, Chen JM. Wang LD. J CO. Util. 2021, 49: 101565
- 24 Zhou YC, Chen ZZ, Gong HX, Wang XS, Chen L, Yu HQ. Chem Eng J, 2024, 481: 148690
- 25 Huang YY, Zhang SN, Chen HX, Zhao LM, Zhang ZJ, Cheng P, Chen Y. *Inorg Chem*, 2019, 58: 9916–9921
- 26 Su XJ, Gao M, Jiao L, Liao RZ, Siegbahn PEM, Cheng JP, Zhang MT. Angew Chem, 2015, 127: 4991–4996
- 27 Yu FS, Li F, Hu JX, Bai LC, Zhu Y, Sun LC. *Chem Commun*, 2016, 52: 10377–10380
- 28 Liu DC, Zhang ML, Huang HH, Feng Q, Su C, Mo A, Wang JW, Qi Z, Zhang X, Jiang L, Chen Z. ACS Sustain Chem Eng, 2021, 9: 9273– 9281
- 29 Guo ZG, Chen G, Cometto C, Ma B, Zhao HY, Groizard T, Chen LJ,

- Fan HB, Man WL, Yiu SM, Lau KC, Lau TC, Robert M. *Nat Catal*, 2019. 2: 801–808
- 30 Ouyang T, Wang HJ, Huang HH, Wang JW, Guo S, Liu WJ, Zhong DC, Lu TB. *Angew Chem Int Ed*, 2018, 57: 16480–16485
- 31 Chandler CJ, Deady LW, Reiss JA, Tzimos V. J Heterocycl Chem, 1982, 19: 1017–1019
- 32 Kounalis E, Lutz M, Broere D. *Chem Eur J*, 2019, 25: 13280–13284
- 33 He C, Lippard SJ. *Tetrahedron*, 2000, 56: 8245–8252
- 34 Nanthakumar A, Fox S, Murthy NN, Karlin KD. J Am Chem Soc, 1997, 119: 3898–3906
- 35 Wang L, Zhou G, Tian Y, Yan L, Deng M, Yang B, Kang Z, Sun H. Appl Catal B-Environ, 2019, 244: 262–271
- 36 Hu C, Tsai WF, Wei WH, Andrew Lin KY, Liu MT, Nakagawa K. Carbon, 2021, 175: 467–477
- 37 Yamazaki Y, Takeda H, Ishitani O. J Photochem Photobiol C-Photochem Rev, 2015, 25: 106–137
- 38 Su XJ, Gao M, Jiao L, Liao RZ, Siegbahn PE, Cheng JP, Zhang MT. Angew Chem Int Ed, 2015, 54: 4909–4914
- 39 Liao LF, Lien CF, Shieh DL, Chen MT, Lin JL. J Phys Chem B, 2002, 106: 11240–11245
- 40 Zhu XW, Huang SQ, Yu Q, She YB, Yang JM, Zhou GL, Li QD, She XJ, Deng JJ, Li HM, Xu H. Appl Catal B-Environ, 2020, 269: 118760
- 41 Wang HF, Wang HJ, Zhong DC, Lu TB. *Proc Natl Acad Sci USA*, 2024, 121: e2318384121
- 42 Huang NY, He H, Liu SJ, Zhu HL, Li YJ, Xu J, Huang JR, Wang X, Liao PQ, Chen XM. *J Am Chem Soc*, 2021, 143: 17424–17430
- 43 Senanayake SD, Stacchiola D, Liu P, Mullins CB, Hrbek J, Rodriguez JA. J Phys Chem C, 2009, 113: 19536–19544